Energy Recovery System for a Universal Robot UR5

Bjarke V. Laustsen, Mads Egekvist, Matias Kjerulf, Mikkel Højfeldt, Oliver Jensen, Rasmus J. Pedersen

Department of Materials and Production, Aalborg University
Fibigerstraede 16, DK-9220 Aalborg East, Denmark
Email: bvla19, megekv18, mkjeru19, mhajfe19, ojense18, rjpe19@student.aau.dk,
Web page: http://www.mechman.mp.aau.dk/

Abstract
The use of robots in the production industry is rising [1] and so is the interest for reducing our carbon footprint by lowering energy consumption [2]. The robotics manufacturer Universal Robots designs robots with an Energy Eater system [3]. This Energy Eater dissipates the generated braking energy as heat. A more energy-efficient method is investigated in this paper, which results in an energy storage unit of multiple supercapacitors. The sizing of the storage unit is based on a worst-case scenario for the UR5 robot. In order to verify the energy unit as a feasible solution for the problem, a controller for the permanent magnet synchronous motor (PMSM) in a UR5 base joint is constructed. The base joint, in pair with the controller, is examined through experiments.

Keywords: Regenerative braking, PMSM, Optimisation, Control, Robotics, Power electronics

1. General Introduction

In the field of industrial robotics, one of the challenges currently faced on the road to greener manufacturing is excessive power consumption [4]. This paper analyses the possibility of implementing an energy recovery system in a UR5 robot arm from Universal Robots. This would replace the currently used system of energy eater modules, a collection of parallel braking resistors. To serve as a platform for developing these systems, a permanent magnet synchronous motor (PMSM) from the base joint of a UR5 has been donated by Universal Robots. Figure 1 shows a CAD model of a UR5 robot with an indication of the base joint location.

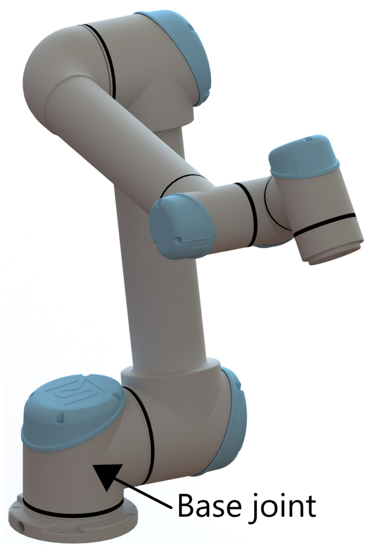

Fig. 1 CAD drawing of a UR5 robot

To further examine this problem, an analysis of possible energy recovery system topologies are presented:

1.1 Topology

During braking operations, electrical energy is generated through induction in the PMSM. This section deals with different topology configurations for harvesting this energy. Topology 1 covers Universal Robots' current configuration.

Topology 1
Generated energy in the DC-bus is stored in electrolytic capacitors, while the rest is directed through the energy eater module and converted into heat. This paper deals with creating a system that would replace this configuration.

Topology 2
Using a bidirectional rectifier, energy generated on the DC-bus from regenerative braking can be converted to AC and delivered back to the grid.

Topology 3
Replacing the energy eater configuration of topology 1 with a supercapacitor circuit would enable short-term storage of the generated energy. A supercapacitor is preferable to a battery, as the charge and discharge rate is greatly increased [5]. Along with supercapacitors, a buck-boost converter would be required for such a system, to control the energy to and from the supercapacitors.

This method is the most attractive topology and will therefore be examined further.

The design process of the regenerative system includes, first of all, an analysis of the energy harvesting problem. For this purpose, studies of hypothetical scenarios of robot arm operation are used to gain insight into possible "worst case" scenarios in which maximum energy storage capacity and energy harvesting and deployment rates are the limiting design factors.

1.2 Worst case

To analyse the required energy storage and charging rate, a case study is introduced. The worst case regarding energy can be seen in figure 2.

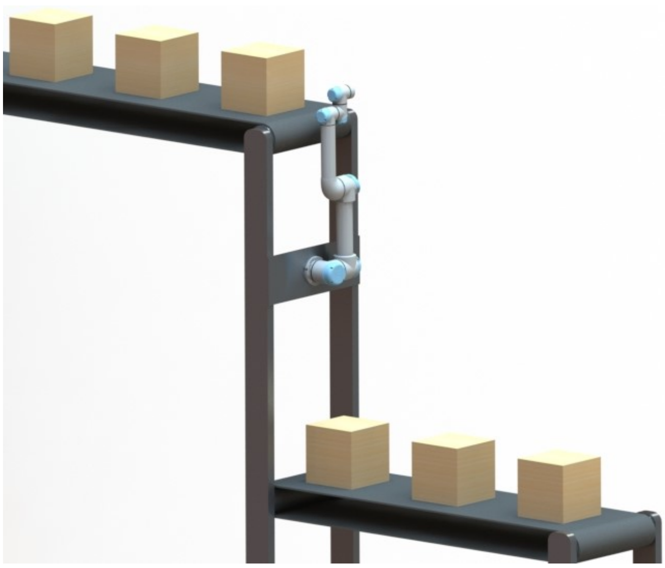

Fig. 2 CAD drawing of worst case.

The goal is to get a power curve that can serve as an input and dimensioning basis for the buck-boost system. This is defined by the acceleration curve.

The shape of the acceleration curve is a square wave, where it will have a constant acceleration until a specific velocity is reached at t_1. From here, it will have an acceleration of zero until it decelerates at t_2 and reaches the desired angle θ_3 at t_3. The angular position θ, angular velocity ω and angular acceleration α are shown in figure 3.

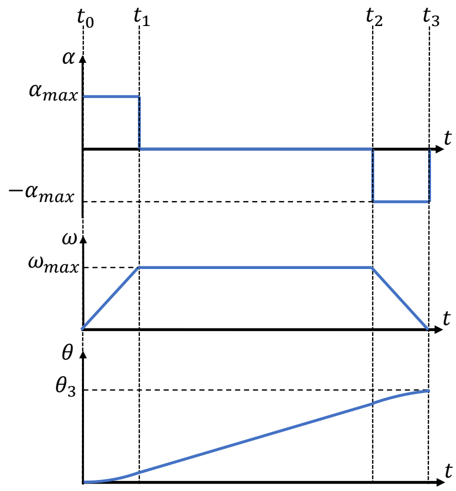

Fig. 3 Motion curve.

Based on this motion curve and the specifications of the robot multiple equations describing the energy and power in the system can be formulated. This results in two worst-case scenarios, one where the captured energy is highest and one where the power is highest. This is due to the fact that the potential energy captured is highest when the robot arm rotates from the topmost position to the lowest position but the power is at its greatest when the robot arm is braked at a 90-degree angle from its topmost position.

The power and energy curves for the worst case when the robot is set to rotate 180 degrees (worst-case 1) can be seen in figure 4 and 5.

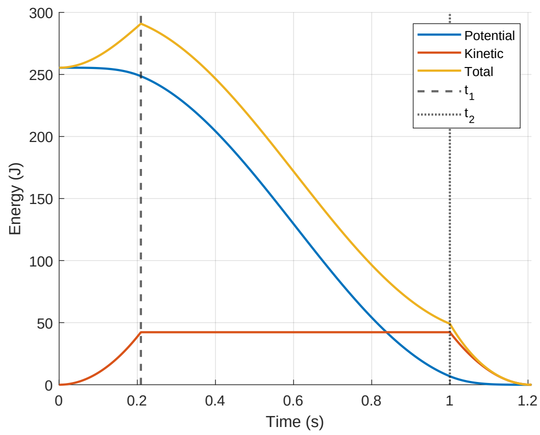

Fig. 4 Energy curve worst case 1.

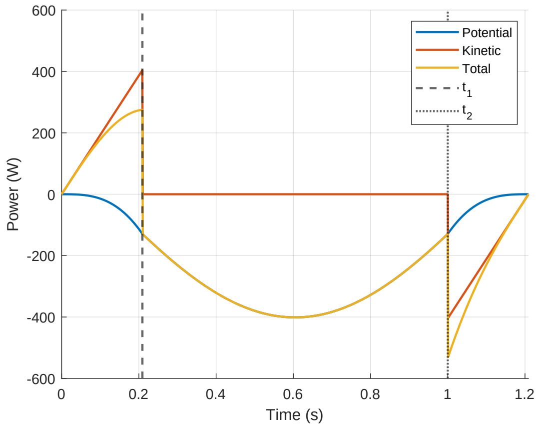

Fig. 5 Power curve worst case 1.

The power and energy curves for the worst case when the robot is set to rotate 90 degrees (worst-case 2) can be seen in figure 6 and 7.

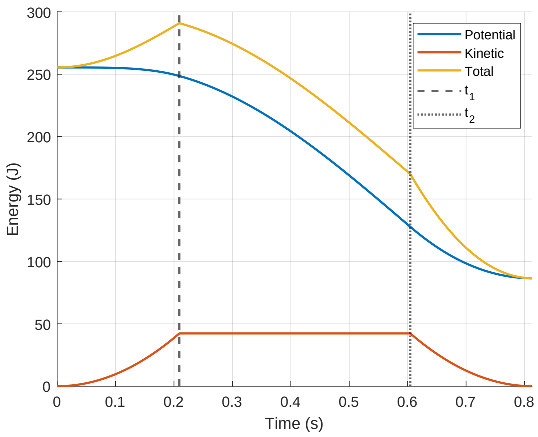

Fig. 6 Energy curve worst case 2.

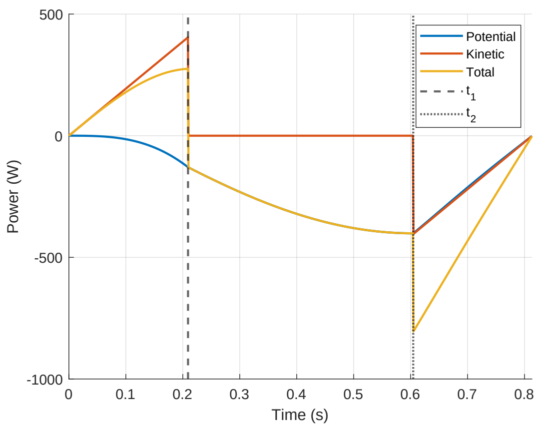

Fig. 7 Power curve worst case 2.

This concludes the problem analysis and a problem statement can now be formulated based on the subjects examined in this chapter.

1.3 Problem statement

With the supercapacitors required storage and recharge rate capabilities determined, a problem statement can be formulated as:

"How can an Energy Recovery System based on the worst case be designed for the PMSM in a UR5-robot"

2. Permanent Magnet Synchronous Motor

In order to inspect motor power dynamics and create an environment for testing and analysing load cases, a simulation model of the electric motor driving the base joint of the UR5 robot is derived throughout this section. [6]

The motor is a three-phase, star-connection PMSM with p surface mounted magnets. A diagram of the stator circuit is seen in figure 8.

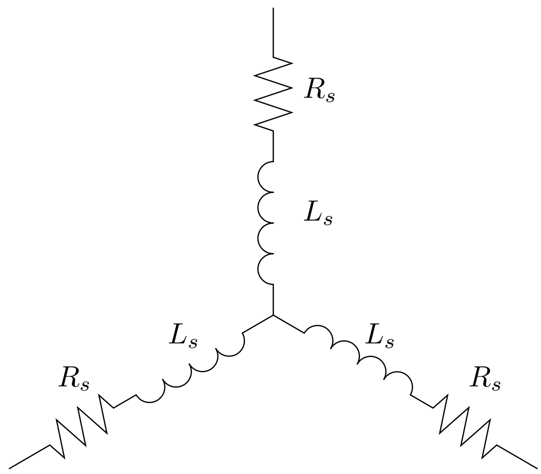

Fig. 8 Circuit diagram of three-phase motor.

Here, L_s and R_s are the stator inductances and resistances, respectively. These are assumed equal for each phase.

The governing equations for the electrical dynamics of the motor are the voltage equations:

$$v_{abc} = R_s i_{abc} + \frac{\mathrm{d}\lambda_{abc}}{\mathrm{d}t} \tag{1}$$

where v, i and λ are the phase voltages, currents and flux linkages, respectively, and the abc subscript denotes vectors containing components for the a, b and c phase.

For control purposes, DC quantities are wanted as opposed to AC quantities. To achieve this, Clarke and Park transformations are utilised. The Clarke transformation projects three-phase quantities onto two orthogonal axes, while the Park transform rotates the reference frame with a given angle θ. Together, they form the transform matrix $T_{dq}(\theta)$:

$$T_{dq}(\theta) = \frac{2}{3}\begin{bmatrix} \cos(\theta) & \cos(\theta-\phi) & \cos(\theta+\phi) \\ -\sin(\theta) & -\sin(\theta-\phi) & -\sin(\theta+\phi) \end{bmatrix}$$

where $\phi = \dfrac{2\pi}{3}$. Picking $\theta = \theta_e$, the electrical angle of the motor, one gets the voltage equations in the synchronously rotating dq reference frame:

$$v_d = R_s i_d + \frac{\mathrm{d}\lambda_d}{\mathrm{d}t} - \omega_e \lambda_q \tag{2}$$

$$v_q = R_s i_q + \frac{\mathrm{d}\lambda_q}{\mathrm{d}t} + \omega_e \lambda_d \tag{3}$$

where $v_{dq} = T_{dq}(\theta_e)v_{abc}$, $i_{dq} = T_{dq}(\theta_e)i_{abc}$ and

$$\lambda_d = L_s i_d + \lambda_{pm} \tag{4}$$

$$\lambda_q = L_s i_q \tag{5}$$

λ_{pm} being the flux linkage due to the permanent magnets. ω_e is the motor electrical frequency, as well as the rate of rotation of the reference frame, and the aforementioned dq variables are thus DC.

The electromechanical torque T_e generated by the motor can be found by considering motor input power:

$$\begin{aligned} P_{in} &= \frac{3}{2} v_{dq}^T i_{dq} \\ &= \frac{3}{2}\left(\underbrace{R_s\left(i_d^2 + i_q^2\right)}_{\text{Copper losses}} + \underbrace{i_{ds}\frac{\mathrm{d}\lambda_d}{\mathrm{d}t} + i_q\frac{\mathrm{d}\lambda_q}{\mathrm{d}t}}_{\text{Magnetic energy variance}} \right) \\ &+ \underbrace{\frac{3}{2}\omega_e \lambda_{pm} i_q}_{\text{Mechanical power}} \end{aligned} \tag{6}$$

As mechanical power is the product of torque and rotor frequency $\omega_r = \dfrac{2}{p}\omega_e$, the mechanical power portion of (6) is divided by rotor frequency yielding:

$$T_e = \frac{3}{2}\frac{p}{2}\lambda_{pm} \tag{7}$$

While T_e is the driving torque of the rotor, several torques act against it. These include the load torque T_L and an assumed friction model of linear viscous friction with coefficient B and coulomb friction with coefficient C_f. Collectively, the rotor dynamics can be modelled through Newtons second law:

$$J\frac{\mathrm{d}\omega_r}{\mathrm{d}t} = T_e - T_L - B\omega_r - C_f sgn(\omega_r) \tag{8}$$

where J is the mass moment of inertia of the rotor.

With a complete PMSM model, the only missing requirement to allow the user to issue motor speed commands is the control system. A Field Oriented Control (FOC) approach is taken, wherein reference rotor speeds are regulated to achieve reference currents, which in turn are regulated to produce reference voltages to be input to the system. A block diagram of the control scheme can be seen in figure 9.

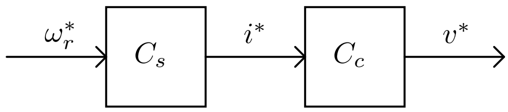

Fig. 9 Block diagram of PMSM control system. $*$-superscript denote reference values.

Here, C_s is a Proportional-Integral (PI) speed controller and C_c is a collection of PI controllers and decoupling feedforward contributions for the d- and q-axis currents. The gains of these controllers are determined based on estimates of motor parameters.

2.1 Parameter estimation

Permanent magnet motors have three different parameters: stator resistance, permanent magnet flux linkage and inductance. The parameters have been estimated through a series of tests. The parameter estimation is done in accordance with [7].

Stator Resistance

The stator resistance is estimated by using a DC-source connected with two multimeters to measure both the voltage over two coils and the current through the coils, with wiring topology similar to the probe 2 and 4 shown in figure 10. A total of 12 measurements were conducted to check all coils and average the measurements. All measurements were conducted over no more than a few seconds, to avoid unaccounted heat generation in the motor, but at steady state. Each coil resistance is found by dividing the calculated circuit resistance by two. The nominal resistance of the motor was determined to be $\sim 0.363\Omega$ per coil.

Stator Inductance

The Stator inductance is approximately constant throughout a full rotation, as the magnets are curved to generate a constant flux at the stator interface. The stator inductance can be experimentally determined by supplying the motor with a DC-current as shown in figure 10. After steady state is reached, the DC-source is disconnected and the response is recorded by an oscilloscope, shown in figure 11.

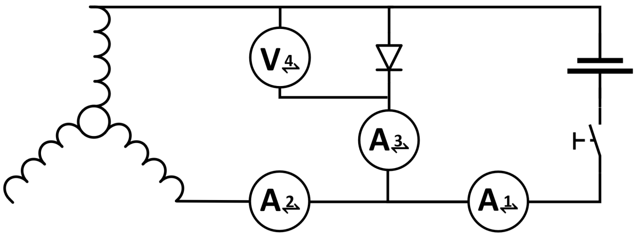

Fig. 10 Test circuit for inductance measurements.

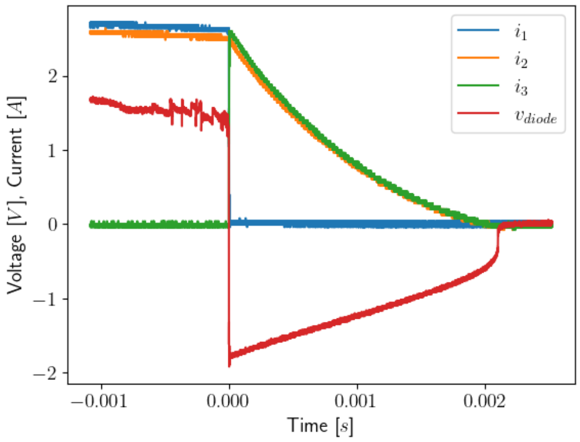

Fig. 11 Recorded currents and voltage of the inductance test.

Based on a first order system response, the inductance can be heuristically approximated in the transient area, with the recorded voltage v_{diode} as input. The inductance was fitted to be $L \approx 0.75\text{mH}$, per coil.

Permanent Magnet Flux Linkage

The permanent magnet flux is determined by driving the motor around at a constant velocity and recording the three phase-to-phase voltages.

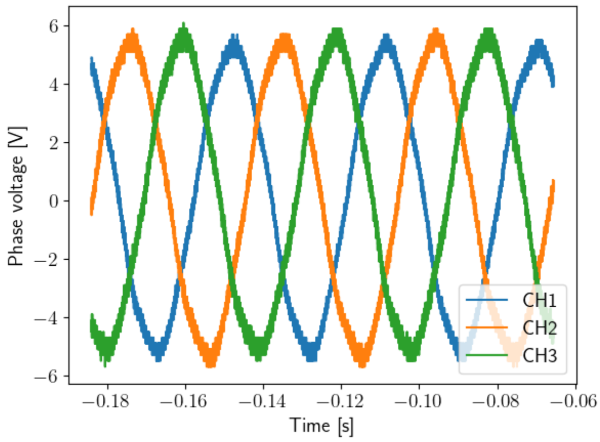

Fig. 12 Back-EMF experiment output voltage.

By inspecting the data, the electrical rotational speed ω_e and the peak back-electromotive-force (back-EMF) voltage $\hat{e}$, can be determined from the length of the sinusoidal periods and the peak voltage values respectively. It should be noted, that the peak voltage values should be divided by $\sqrt{3}$ in order to obtain phase-to-neutral values, and thus:

$$\hat{\lambda}_{pm} = \frac{\hat{e}}{\sqrt{3}\omega_e} = \frac{5.9V}{\sqrt{3} \cdot 157rad/s} = 0.021V/rad/s \tag{9}$$

3. Buck-boost converter

It is of interest to transfer the power from the PMSM to the supercapacitors when it works as a generator, and back again when it works as a motor. In order to transfer the energy to the supercapacitors and back again, a buck-boost converter is introduced. The topology is seen in figure 13. [8]

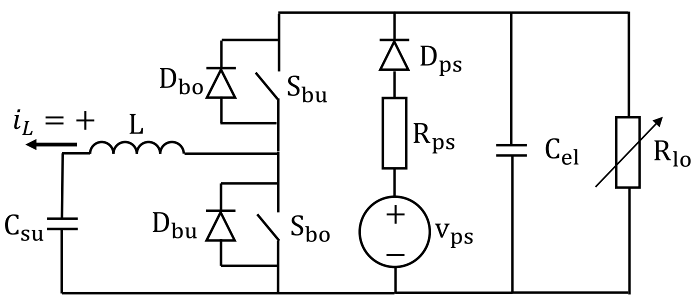

Fig. 13 Buck-boost converter.

The circuit consists of a constant voltage source from the power supply v_{ps}, a small current limiting resistor R_{ps}, a diode that ensures current can only flow from the voltage source D_{ps} and an electrolytic capacitor to smooth out the voltage ripples C_{el}. Together, these components are what will be modelled as the "DC-bus", where the bus is the voltage measured across the electrolytic capacitor, and these components are predetermined by existing technology. The goal is to determine the dimensioning of the supercapacitors with a capacitance of C_{su}, the inductor with an inductance of L, the switches S_{bu}, S_{bo} and the diodes D_{bu}, D_{bo}. The buck-boost system will be operated as a synchronous buck-boost converter, where if one switch is closed the other is open. This will increase efficiency and simplify the control scheme.

Figure 14 shows the PWM signal consisting of the buck switch ON-time, shown in blue, and the OFF-time, shown in orange, all defined from the independent duty cycle D and the constant value for the switching frequency f_{sw}.

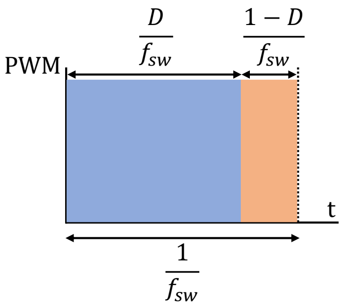

Fig. 14 Illustration of duty cycle.

The differential equations of the system

A way to design a controller, which outputs a duty cycle, is to establish the differential equations for the system, which describe how the currents and voltages change based on different inputs. The system has three states: The current through the inductor i_L, the voltage across the supercapacitor $v_{C,su}$ and the voltage across the electrolytic capacitor $v_{C,el}$. The differential equations change depending on which switch is open, and to analyse them based on the duty cycle, an average is taken [9]. The equations are established from utilising Kirchhoff's voltage and current laws.

Algebraic Equations

$$i_{ps} = \begin{cases} \frac{v_{ps}-v_{C,el}}{R_{ps}} & \text{if } v_{ps} \geq v_{C,el} \\ 0 & \text{if } v_{ps} < v_{C,el} \end{cases} \tag{10}$$

$$v_{C,el} = v_o \tag{11}$$

Differential Equations

$$\frac{\mathrm{d}i_L}{\mathrm{d}t} = \frac{1}{L}(Dv_{C,el} - R_{tot}i_L - v_{C,su}) \tag{12}$$

$$\frac{\mathrm{d}v_{C,su}}{\mathrm{d}t} = \frac{1}{C_{su}}i_L \tag{13}$$

$$\frac{\mathrm{d}v_{C,el}}{\mathrm{d}t} = \frac{1}{C_{el}}\left(i_{ps} - Di_L - \frac{P_{motor}}{v_o}\right) \tag{14}$$

Linearisation of the differential equations

The purpose of operating the system as a buck converter is to capture the power from the motor. In this scenario, the power supply should output $0\mathrm{A}$ of current, and therefore the variable i_{ps} is set to zero for this analysis. The natural step from here is to linearise the equations and develop a linear controller based on the linear system, and this is done by neglecting $v_{C,su}$ as a state, but including it as a disturbance. This will transform the equations to two differential equations, which will then be linearised around a point of equilibrium. This can be written in state space form seen in equation 15.

$$\begin{bmatrix} \frac{\mathrm{d}i_L}{\mathrm{d}t} \\ \frac{\mathrm{d}v_{C,el}}{\mathrm{d}t} \end{bmatrix} = \begin{bmatrix} -\frac{R_{tot}}{L} & \frac{D_0}{L} \\ -\frac{D_0}{C_{el}} & \frac{P_{motor0}}{v_{C,el0}^2 C_{el}} \end{bmatrix} \begin{bmatrix} i_L \\ v_{C,el} \end{bmatrix} + \begin{bmatrix} \frac{v_{C,el0}}{L} \\ -\frac{i_{L0}}{C_{el}} \end{bmatrix} D + \begin{bmatrix} 0 & -\frac{1}{L} \\ -\frac{1}{v_{C,el0}C_{el}} & 0 \end{bmatrix} \begin{bmatrix} P_{motor} \\ v_{C,su} \end{bmatrix} \tag{15}$$

Linearisation should also be done for the boost converter, but this process is not considered to be within the scope of this paper.

Controller design

The following text is loosely based on the book [10]. When the motor is working as a generator, voltage over the electrolytic capacitors needs to be kept somewhat constant to capture the power coming from the motor. Therefore, the main state to control is the electrolytic capacitor.

When the motor is consuming power again, the supercapacitors need to either charge or discharge based on whether they are below or above the reference voltage. Therefore the main state to control is the supercapacitor voltage.

In both cases, the inductor current needs to be kept under 30A at all times and is, therefore, a second state to control in both cases. A way to implement this control strategy in both cases is to establish feedback through cascaded loops, where the current reference is generated based on the states of both voltages combined with saturation on the current reference. The block diagram showing the final control scheme, without saturation, is depicted in figure 15.

and the output seen on equation 16.

$$v_{C,el} = G_{ref}v_{C,el,ref} + G_{dist1}v_{C,su} + G_{dist2}P_{motor} \tag{16}$$

These transfer functions are visualised through the magnitude of their bode plot on figure 17.

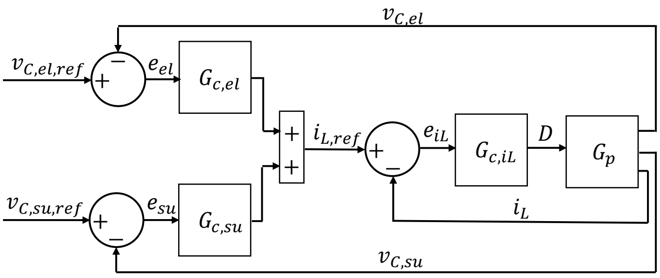

Fig. 15 Block Diagram of buck-boost control scheme.

When having cascaded loops, the inner controller is designed first and afterwards the outer controller is designed. The inner transfer function is between the duty cycle and the inductor current, where the outer transfer function is between the current and the electrolytic capacitor voltage (in buck operation).
The controller for the inner loop $G_{C,iL}$ is selected as a PI controller, since the inner transfer function has a zero in the origin. The PI controller is tuned by using loop shaping on the open loop transfer function with the objective of decreasing the effect of the zero in the origin, and having a phase margin of 60°. Figure 16 shows the open loop transfer function with different gains, where the final is the yellow transfer function. The same method is used for the outer loops, where

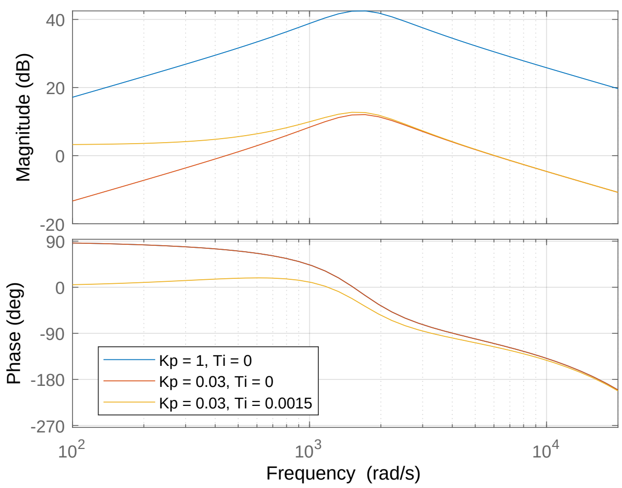

Fig. 16 Loop Shaping inner Loop.

the result is a simple proportional controller for both voltages.
Additionally, from the state space equations and the controller equations the disturbance rejection can be analysed. This done by firstly finding the the transfer functions, which describes the input/output relationship between the output state and the input disturbance variable, and then the input/output from the reference

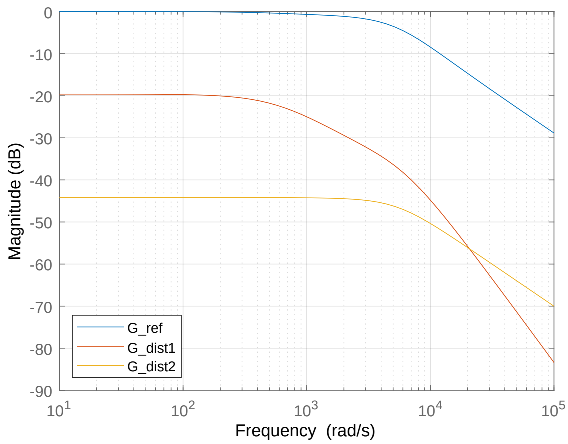

Fig. 17 Disturbance rejection and reference tracking.

Here, the closed loop transfer function has a bandwidth of $4516\frac{\text{rad}}{\text{s}}$, and the disturbance transfer functions are below -20dB for all frequencies, which implies good disturbance rejection.

Final remarks
From here, the PI controller is discretised to realise the control on a microcontroller. Additionally, anti-windup is implemented in the control scheme. This is then tested in a simulation to verify that the electrolytic capacitor voltage stays somewhat constant, and that the super capacitors will stay around a fixed point over various cycles of the robot.

4. Laboratory setup

With the modelling of the buck-boost system as well as the PMSM finalised, a laboratory setup is now constructed.

4.1 Mechanical setup

This subsection describes the full mechanical setup including multiple analyses to determine the strength of each part. The mechanical test setup can be seen in figure 18.

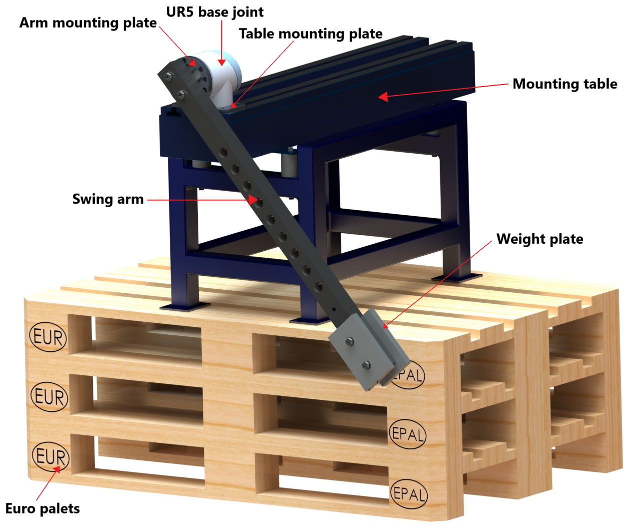

Fig. 18 CAD drawing of lab setup.

The test setup consists of five major segments: (1) Three Euro pallets to increase the height of the setup. (2) The mounting table to mount the UR5 to, and increase stability. (3) The base joint PMSM from a UR5 robot. (4) Two mounting plates. (5) A swing arm with two weight blocks. The swing arm and the weight blocks are designed such that their weight and mass moment of inertia matches the real robot arm under full extension and loading.

4.2 Programming

For implementing the PMSM FOC scheme, a C program is written for the STM32 microprocessor. Along with the microprocessor, a motor control extension board is utilised.

Hardware
The motor control board features a dedicated encoder slot, a voltage divider for DC-bus sampling and three shunts for sampling the three-phase current. The motor control board is equipped with six MOSFETs for converting $48\,\mathrm{V}$ DC into three-phase AC.[11]

Sampling states
The voltage and currents are sampled with two analog-to-digital converters (ADCs) and the data is transferred through direct memory access (DMA) to minimise the strain on the CPU. The encoder is sampled using STMs encoder mode feature.

For velocity estimation, a timer is configured to send a fixed interrupt. When an interrupt is flagged, the difference in encoder pulses is compared, and velocity is estimated.

Driving signals
The PMSM is actuated by sending gating pulses to the six MOSFETs contained in figure 19. The MOSFETs

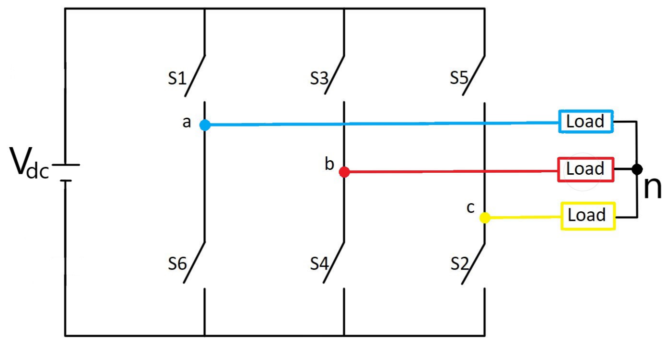

Fig. 19 Three-phase inverter sketch.

are configured in pairs using a timer with three-channel complementary PWM. As such when S1 is closed, S6 is open.

To avoid a short circuit between the pairs, a $500\,\mathrm{ns}$ dead time is configured for each channel.

The timers switching frequency is $10\,\mathrm{kHz}$ in up-down counting. In accordance with [12], up-down counting is used. This is often the case for AC-motor control due to reduced harmonic distortion and switching noise. The timer is synchronised with the ADCs trigger, as the three-phase current readings should occur when MOSFETs are closed.

Space Vector Pulse Width Modulation
For determining the duration of the duty cycles for the three PWM channels, Space Vector Pulse Width Modulation (SVPWM) is utilised. This section is based on [6]. SVPWM is chosen as it produces a $15.5\,\%$ higher fundamental output than sine-triangle PWM (SPWM), which is another popular method for PWM conversion. A block diagram of the SVPWM method is contained in figure 20. The method uses the v_α, v_β voltage vector

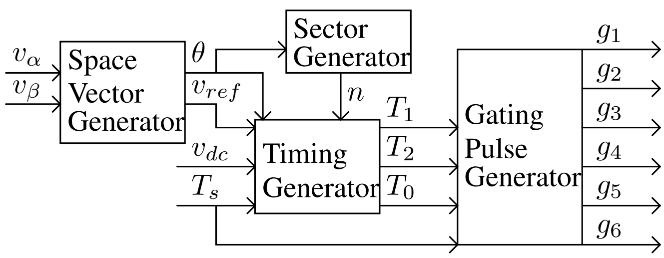

Fig. 20 Block diagram of SVPWM.

from FOC to construct a rotating reference voltage vector. The vector is depicted in figure 21.

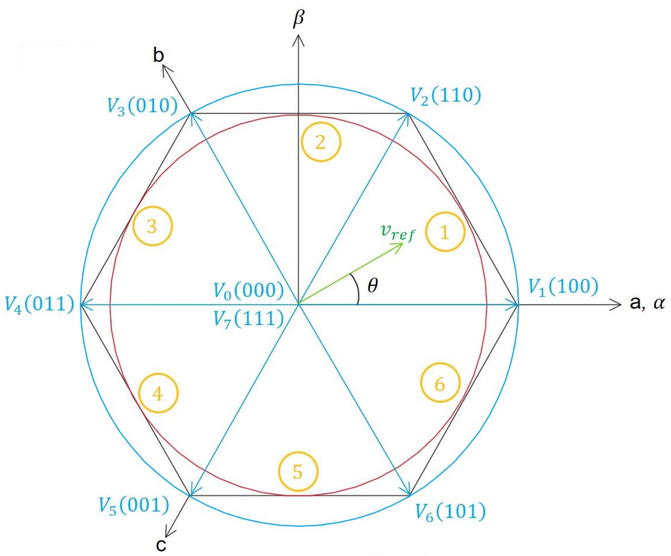

Fig. 21 SVPWM representation in the $\alpha\beta$-coordinate system. Red circle is SPWM and blue circle SVPWM.

The sector generator determines in which sector, V_1 through V_6, the voltage vector is located, while the timing generator determines the duration of the duty cycle.

The timing equations are:

$$T_1 = \sqrt{3}\frac{|v_{ref}|}{v_{dc}}T_s \sin\left(\frac{n\pi}{3} - \theta\right)$$

$$T_2 = \sqrt{3}\frac{|v_{ref}|}{v_{dc}}T_s \sin\left(\theta - \frac{(n-1)\pi}{3}\right)$$

$$T_0 = T_s - (T_1 + T_2)$$

Here v_{ref} is the reference voltage vector, T_s is the switching period, v_{dc} DC-bus voltage, n is the sector number and θ is the voltage vectors absolute angle.

Table I, contains the duty cycle determination for sector 1.

Sectors	**Upper Switches ON-time**
Sector 1	$S_1 = T_1 + T_2 + \frac{T_0}{2}$ $S_3 = T_2 + \frac{T_0}{2}$ $S_5 = \frac{T_0}{2}$

Tab. I Sector 1 switch ON-time.

Align and safety

Overcurrent protection is added in the C program to protect the hardware.

As the FOC scheme is constructed with the assumption that the d axis is aligned with the v_α axis, an align function is added to the C program, which aligns these axes upon startup.

5. Experiments

Through heuristic tuning of the control parameters, the following result, see figure 22, was obtained with a 10 Hz rotor velocity step.

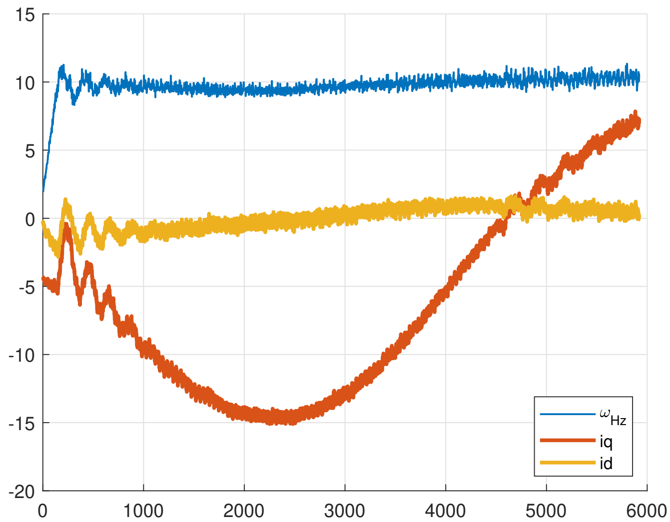

Fig. 22 FOC algorithm 10 Hz step with wcc = 5 and wcs = wcc/1.

The i_d current remains around the zero reference, with some oscillatory behaviour. Noticeably, the velocity remains around the 10 Hz, even when surpassing the upmost vertical position. The upmost vertical position is reached, approximately, where the i_q current crosses the zero axis. As i_q is the torque-producing component, a switching in signs indicates a switch from acceleration to deceleration.

Furthermore, positive i_q implies energy generation, so for future work, the developed energy recovery system should be examined by running this energy through it, instead of the braking resistors.

Further analysis can be made by inspection of oscilloscope readings. Figure 23 and 24 show oscilloscope readings of currents and voltages during motor and generator mode, respectively.

The oscilloscope shows the three phase currents, shown in cyan, pink and yellow, and voltage, shown in green. The voltage is seen to consist of a PWM signal, while the currents are continuous due to the filtering effects of the motor inductance. Furthermore, figure 23 shows the voltage leading the cyan-current in motor mode and figure 24 depicts a phase shift of 180° between the voltage and the cyan-current in generator mode.

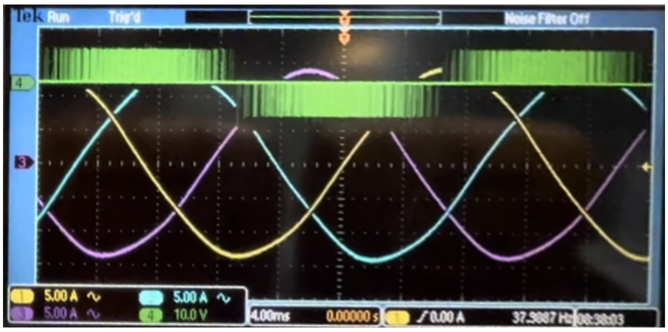

Fig. 23 Currents and voltage during the motor mode.

Fig. 24 Currents and voltage during generator mode.

It can also be seen, that the voltage is more dense in motor mode than in generator mode. This is assumed to be from the friction force and cobber losses essentially producing a braking torque.

Figure 25 is a QR code linking to a youtube video showing the laboratory set-up taking one full revolution with FOC control. Please note the starting "wiggle" (approx 3 sec into the video) of the arm which is the align function running as described earlier.

Fig. 25 A link to a video of the laboratory setup moving with FOC.
Link: https://rb.gy/di31u

6. Conclusion

The problem statement was to investigate

"How can an Energy Recovery System based on the worst case be designed for the PMSM in a UR5-robot"

This was investigated by first developing PMSM and buck-boost models of the system, and designing a controller for these models.
Then, a laboratory setup was designed and constructed to simulate the worst-case scenario.
Afterwards, a PCB for the buck-boost energy recovery system was designed and built, but not tested.
The motor control scheme was then implemented onto the STM32F446 NUCLEO-64 development board with an X-NUCLEO-IHM08M1 motor drive expansion board.
Experiments were conducted and ω_{hz}, i_d as well as i_q control was achieved at low-velocity step commands. With the mechanical arm crossing the topmost vertical position, the i_q graph showed a generated energy. With future work and the implementation of the Buck-Boost system, this energy should be stored in the supercapacitors instead of running across braking resistors.

Acknowledgement
The authors of this work gratefully acknowledge Grundfos for sponsoring the 11th MechMan symposium.

References

[1] IFR, "Ifr international federation of robotics," IFR presents World Robotics 2021 reports, 2021.
[2] U. Nations, "For a livable climate: Net-zero commitments must be backed by credible action," 2022. Accessed: 20/02/2023.
[3] U. Robots, "Service manual, 9.6.94," 2022. Accessed: 20/02/2023.
[4] IEA, "Industry," 2022. Accessed: 11/05/2023.
[5] "The major differences between super capacitors and batteries," 2022. Accessed: 13/02/2023.
[6] S.-H. Kim, Electric Motor Control. Elsevier, 1st ed., 2017.
[7] V. Bobek, "Pmsm electrical parameters measurement," 2013.
[8] "Power topologies handbook," 2023.
[9] "Simulation of a bidirectional dc-dc boost converter using a state-space averaged model," 2017.
[10] C. L. Phillips and J. M. Parr, Feedback Control Systems. Pearson Education, Inc., 2011.
[11] STMicroelectronics, "Low-voltage bldc motor driver expansion board based on stl220n6f7 for stm32 nucleo," 2017. Accessed: 08/02/2023.
[12] A. S. Lab, "Pulse-width modulation (pwm)," s.d. Accessed: 05/05/2023.